Supplement of Atmos. Chem. Phys., 17, 11209–11226, 2017
https://doi.org/10.5194/acp-17-11209-2017-supplement

Atmospheric Chemistry and Physics
Open Access

Supplement of

Sulfate geoengineering impact on methane transport and lifetime: results from the Geoengineering Model Intercomparison Project (GeoMIP)

Daniele Visioni et al.

Correspondence to: Daniele Visioni (daniele.visioni@aquila.infn.it)

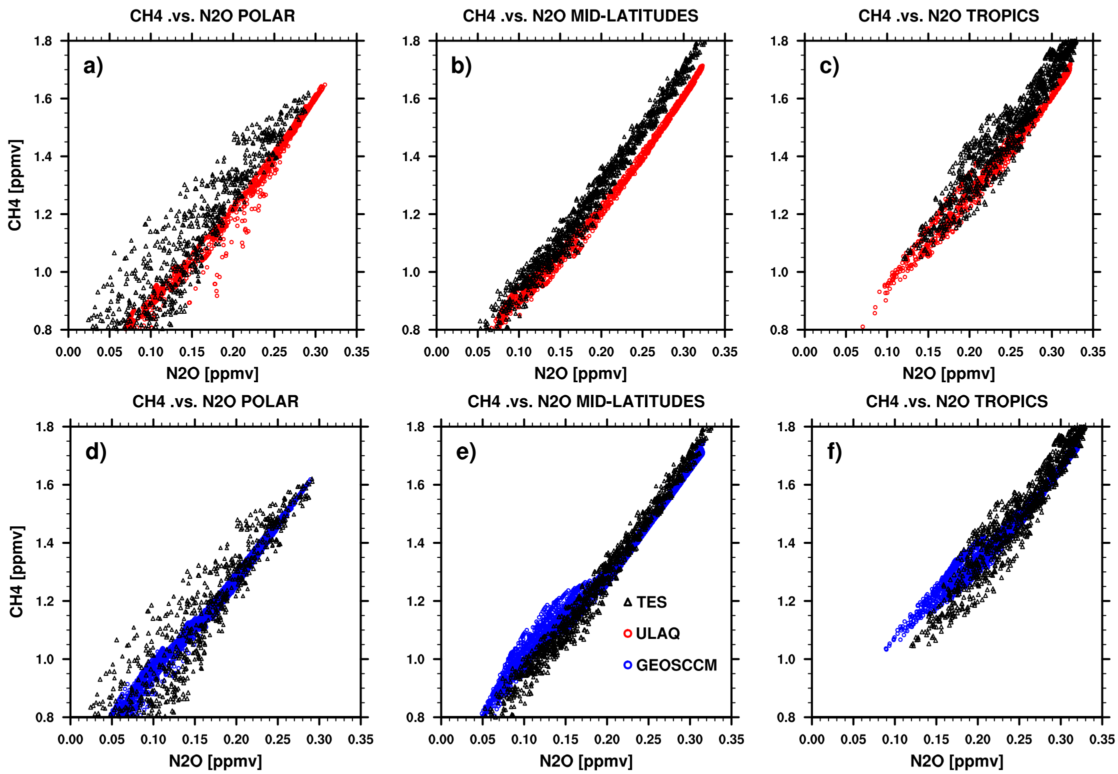

Figure S1. Scatter plots of zonal and monthly mean mixing ratio values of CH_4 and N_2O for ULAQ-CCM (red) and GEOSCCM (blue) simulations, in the layer 1-100 hPa and averaged over 2004-2010. The panels refer to latitude bands (a) and (d) 60S-90S and 60N-90N, (b) and (e) 30S-60S and 30N-60N, and (c) and (f) 30S-30N. Model values are evaluated with CH_4 and N_2O data from TES observations (black), averaged over 2004-2010. The existence of mixing barriers at the edge of the tropical pipe allows the distinction between tropics (panels (c) and (f)) and mid-latitudes (panels (b) and (e)). In polar regions (panels (a) and (d)), models display a more compact correlation compared with observed data: this happens because the latter are affected by a large uncertainty due to low sensitivity of the retrieval method, as shown by Worden et al. (2012) for TES.

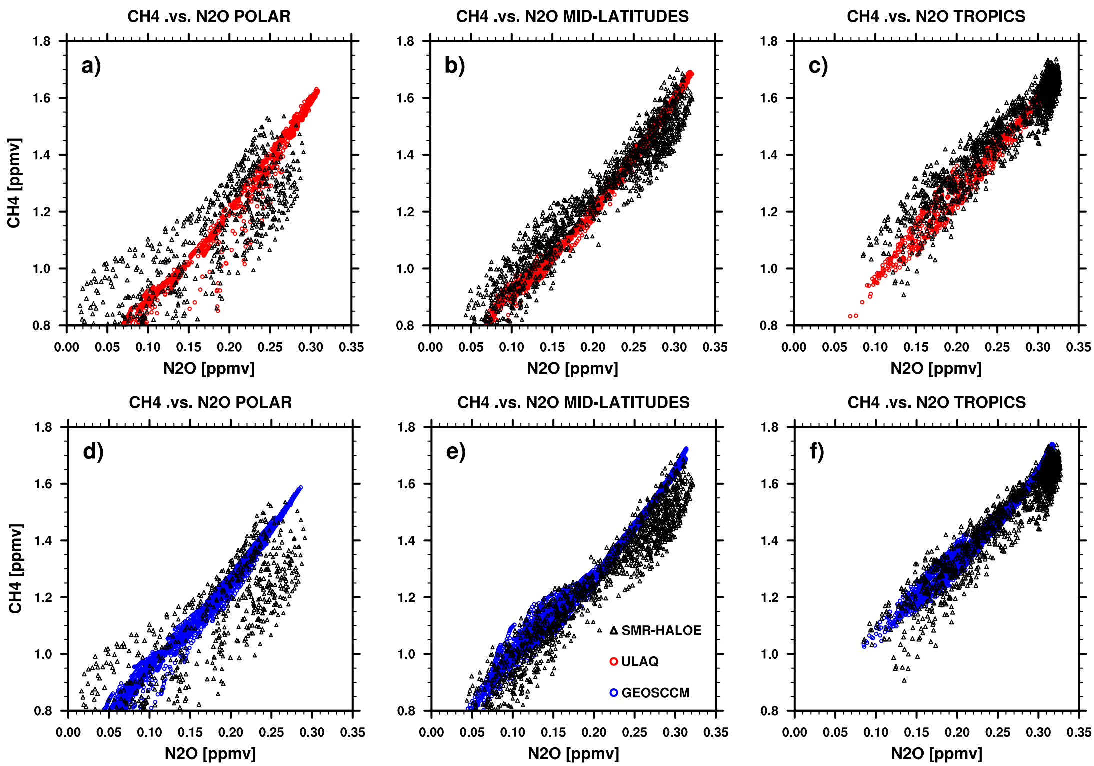

Figure S2. Scatter plots of zonal and monthly mean mixing ratio values of CH_4 and N_2O for ULAQ-CCM (red) and GEOSCCM (blue) simulations, in the layer 1-100 hPa and averaged over 2004-2010. The panels refer to latitude bands (a) and (d) 60S-90S and 60N-90N, (b) and (e) 30S-60S and 30N-60N, and (c) and (f) 30S-30N. Model values are evaluated with CH_4 and N_2O data from HALOE for CH_4 (average 1991-2005) and SMR-Odin for N_2O (average 2001-2005) (Urban et al. (2009)). Model data are averaged over 1991-2005 for CH_4 and 2001-2005 for N_2O. The existence of mixing barriers at the edge of the tropical pipe allows the distinction between tropics (panels (c) and (f)) and mid-latitude (panels (b) and (e)). In polar regions (panels (a) and (d)), models display a more compact correlation compared with observed data due to sparse coverage of the HALOE satellites data, as shown by Grooss and Russell III (2005).

Table S1. a) Pearson correlation coefficient with associated confidence interval calculated using the Fischer transform inverse, for observations and model data presented in Fig. S1 (2004-2010). b) as in a) but for the data presented in Fig. S2 (1991-2005 for the models and HALOE, 2001-2005 for SMR). Overall values in (a) present a better correlation with respect to values in (b): this might be a consequence of a different range of years used for CH_4 (1991-2005) and N_2O (2001-2005) in HALOE and SMR, respectively.

a)					
R_Pearson	90S-60S	60S-30S	30S-30N	30N-60N	60N-90N
TES	0.921 [0.908-0.933]	0.988 [0.986-0.990]	0.971 [0.967-0.974]	0.995 [0.994-0.995]	0.956 [0.948-0.962]
GEOSCCM	0.982 [0.980-0.984]	0.992 [0.990-0.992]	0.990 [0.989-0.990]	0.997 [0.997-0.997]	0.994 [0.994-0.995]
ULAQ-CCM	0.990 [0.988-0.991]	0.996 [0.995-0.996]	0.995 [0.994-0.995]	0.997 [0.997-0.998]	0.993 [0.992-0.994]
b)					
HALOE/SMR	0.761 [0.723-0.794]	0.958 [0.951-0.963]	0.952 [0.947-0.957]	0.970 [0.966-0.995]	0.926 [0.914-0.938]
GEOSCCM	0.978 [0.976-0.980]	0.990 [0.989-0.991]	0.990 [0.989-0.991]	0.996 [0.996-0.997]	0.995 [0.994-0.995]
ULAQ-CCM	0.982 [0.979-0.985]	0.995 [0.994-0.995]	0.993 [0.992-0.993]	0.996 [0.995-0.997]	0.992 [0.991-0.993]

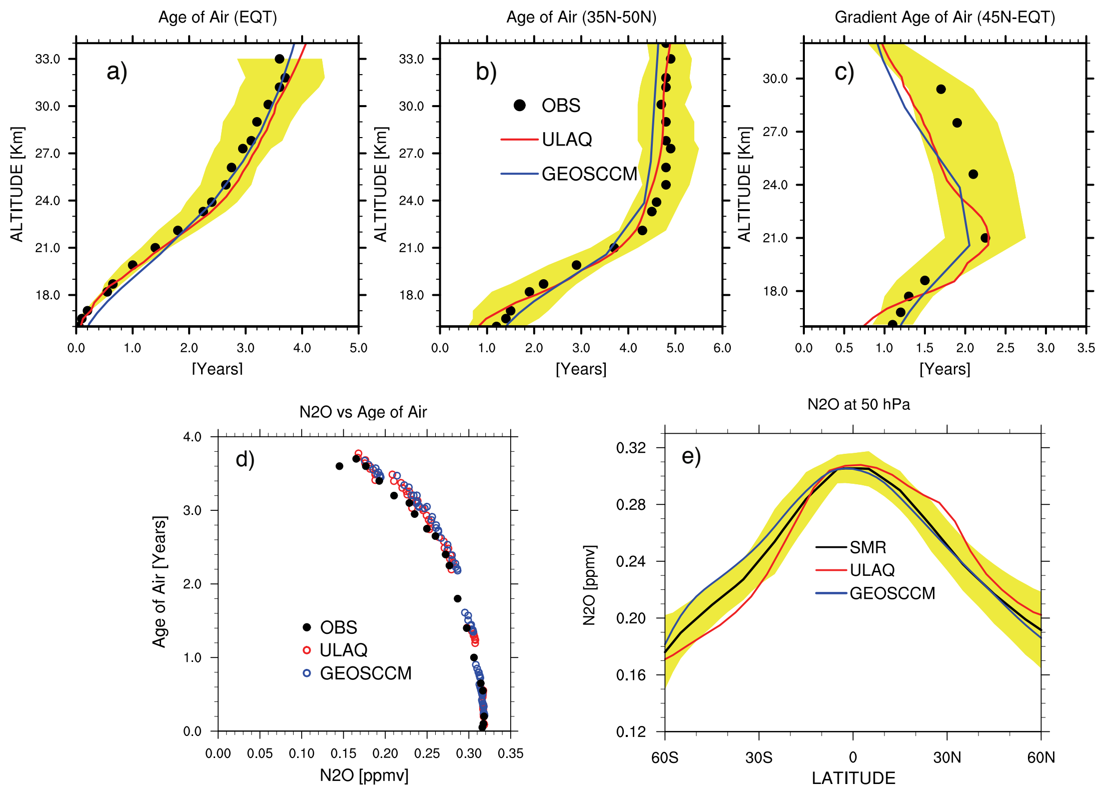

Figure S3. Panels (a,b): vertical profiles of (a) equatorial and (b) mid-latitude AoA for GEOSCCM (blue line) and ULAQ-CCM (red line), compared with the range of observations from Andrews et al. (2001) and Engel et al. (2009) (yellow-filled area). The time average is from 1980 to 2000; the latitudinal average is 10S-10N in (a) and 35N-50N in (b). The latitudinal gradient of AoA is shown in panel (c), calculated as the difference between the Northern Hemisphere mid-latitudes and the equator (symbols and colors are as in panels (a,b)). Panel (d): scatter plot of AoA (years) versus the N_2O mixing ratio (ppmv), for GEOSCCM (blue circles), ULAQ-CCM (red circles) and the median of AoA observations from Andrews et al. (2001) and Engel et al. (2009) versus N_2O SMR observations (black circles). Model values of mean AoA and N_2O shown in this panel represent the climatological mean (1980-2005) in the range 10-100 hPa and 10S-10N; observed values of mean AoA are the same as in panel (a); observed values of N_2O are the SMR/Odin climatological mean (2001-2005). Panel (e): 50 hPa latitudinal section of the N_2O mixing ratio (ppbv) from the same models and observations as in panel (d). The yellow-filled area show the range of time variability of SMR measurements (i.e., $\pm 2\sigma$). Tropical mean AoA profiles (panel a) combine the effect of ascent rate and horizontal mixing. The horizontal gradient of mean age (panel c) isolates the ascent contribution (Strahan et al. (2011)).

Table S2. Parameters of the linear fit of polar temperatures versus eddy heat fluxes (Austin et al. (2003)). The four columns show the correlation between the heat flux at 100 hPa averaged over 40°N to 80°N for January and February versus temperatures at 50 hPa averaged over 60°N to 90°N for February and March in the Northern Hemisphere, while for the Southern Hemisphere the heat fluxes at 100 hPa are averaged between 40°S and 80°S in July and August and the temperatures at 50 hPa are averaged between 60°S and 90°S in August and September. For years 1981-2002, the four columns represent the correlation coefficient between data and their linear fit (first column) and the parameters of this fit (T_0, slope β and standard error σ for the calculation of β, respectively for columns 2,3 and 4).

Northern Hemisphere	R	T_0	β	σ
ERA40	0.69	193.8	1.44	0.27
GEOSCMM	0.80	193.5	1.65	0.22
ULAQ-CCM	0.65	192.8	1.29	0.15
Southern Hemisphere	R	T_0	β	σ
ERA40	0.83	188.7	1.04	0.17
GEOSCMM	0.81	179.3	2.05	0.32
ULAQ-CCM	0.93	185.4	1.76	0.29

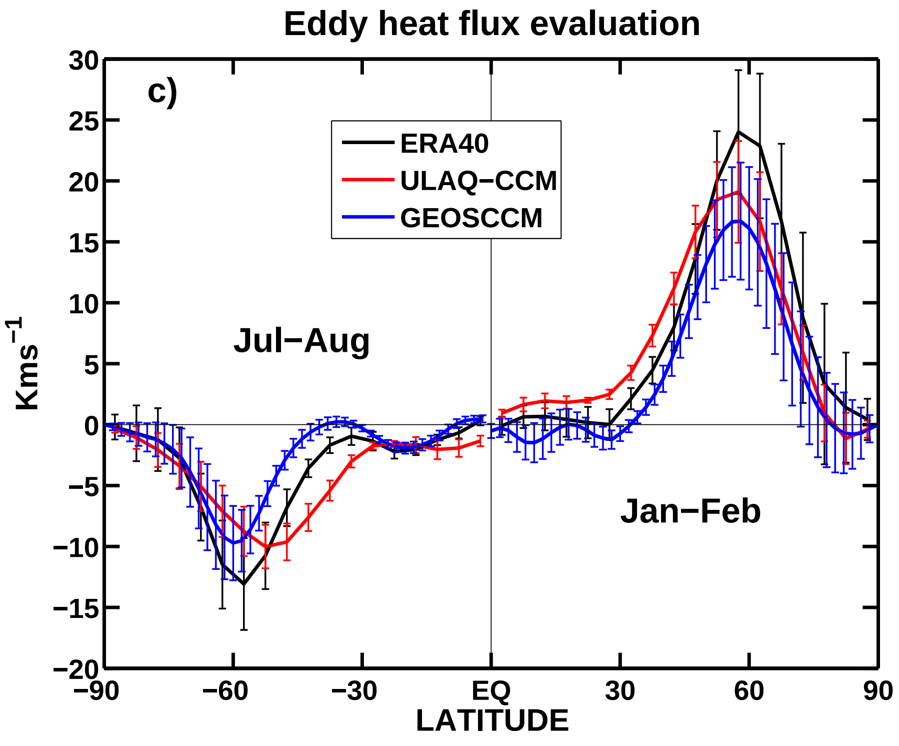

Figure S4. Evaluation of 100 hPa horizontal eddy heat fluxes (in kg km^{-2} yr^{-1}) as a function of latitude averaged over 1981-2002 for the two models (GEOSCCM in blue and ULAQ-CCM in red) with ERA40 reanalysis (Kms^{-1}). The eddy heat fluxes are averaged over winter months, i.e., for July and August in the Southern Hemisphere and January-February over the Northern Hemisphere and are defined as [vT], where v is the 3D meridional wind component and T the temperature. The square brackets [] denote a zonal average and the prime a deviation from the zonal average. Both models fall inside $\pm$ 1σ of the ERA 40 variability from 50° to 90° in both hemispheres.

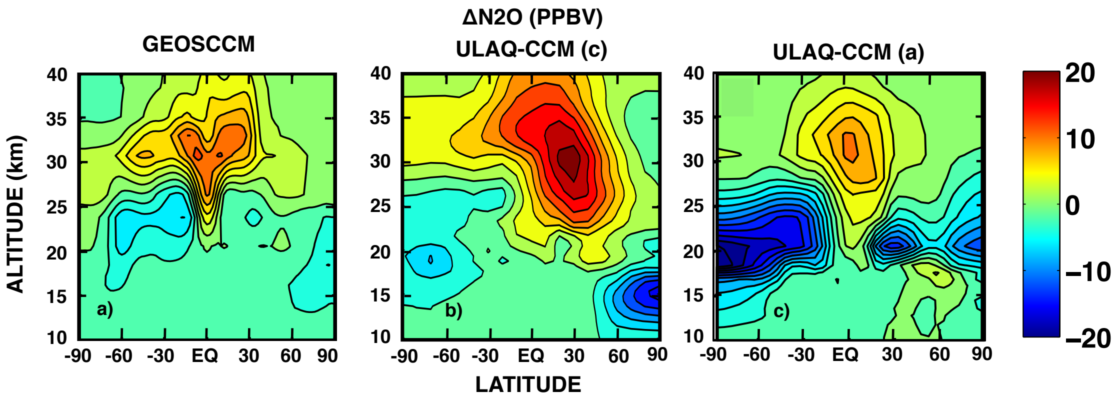

Figure S5. N_2O anomalies for GEOSCCM (panel a), ULAQ-CCM experiment (c) (panel b) and ULAQ-CCM experiment (a) (panel c). This comparison is the same as in Fig. 5, but with the addition of ULAQ-CCM experiment (c) that helps highlighting how changing SSTs in G4 with respect to the control case RCP4.5 may significantly impact the lower stratospheric horizontal mass fluxes and hence the anomalies of long-lived species.

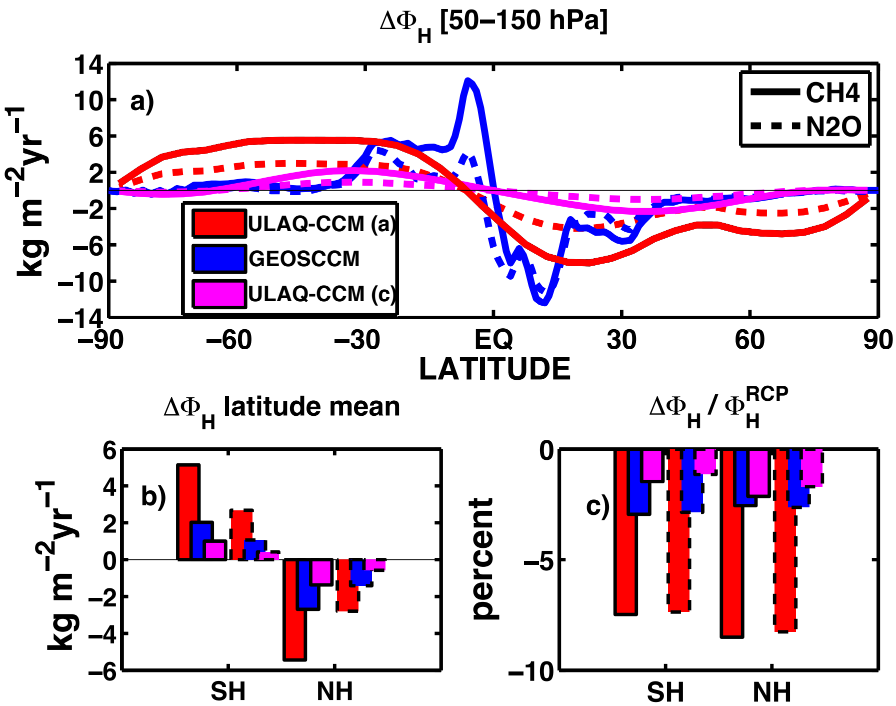

Figure S6. Panel (a): latitude dependent CH_4 (solid line) and N_2O (dashed line) horizontal mass flux anomalies G4-RCP4.5 from the ULAQ-CCM (a), ULAQ-CCM (c) and GEOSCCM calculations, in red, magenta and blue respectively (vertical average 50-150 hPa; time average 2040-2049). Units are kg km^{-2} yr^{-1}. Panels (b) and (c) show the corresponding latitude averaged mass flux anomalies (absolute and percent values, respectively): SH from 90S to 20S; NH from 20N to 90N. The horizontal flux anomalies $\Delta\Phi_H$ are defined as $\Delta[\mathrm{v}\rho_{CH4}]$ and $\Delta[\mathrm{v}\rho_{N2O}]$, where v is the 3D meridional wind component, ρ_{CH4} and ρ_{N2O} are the mass concentrations of CH_4 and N_2O, respectively, and Δ denotes the G4-RCP4.5 difference. As in Fig. S5, this helps clarifying that changing SSTs are the main driver for decreased lower stratospheric horizontal mass fluxes, which in turn produce less export of CH_4 and N_2O from the tropical pipe towards mid-high latitudes.

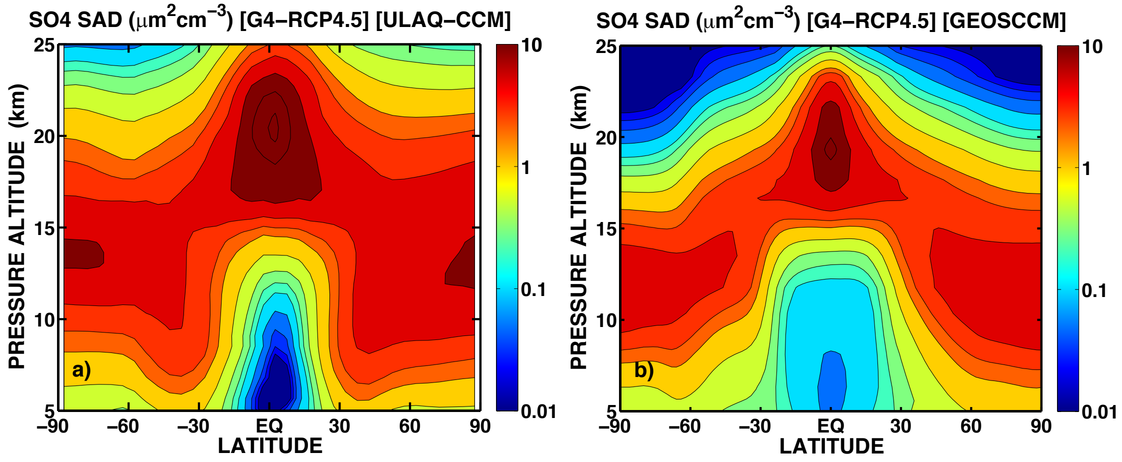

Figure S7. G4-RCP4.5 anomalies of sulfate aerosol surface area density in the troposphere and lower stratosphere up to 25 km altitude, from ULAQ-CCM (panel a) and GEOSCCM (panel b) (time average 2040-2049). Both models show a good confinement of the sulfate aerosol particles in the lower stratospheric tropical pipe. ULAQ-CCM results are from numerical experiments (c) in Table 1. Units are $\mu m^2 cm^{-3}$. The contour line increment is logarithmic (three contours per decade)

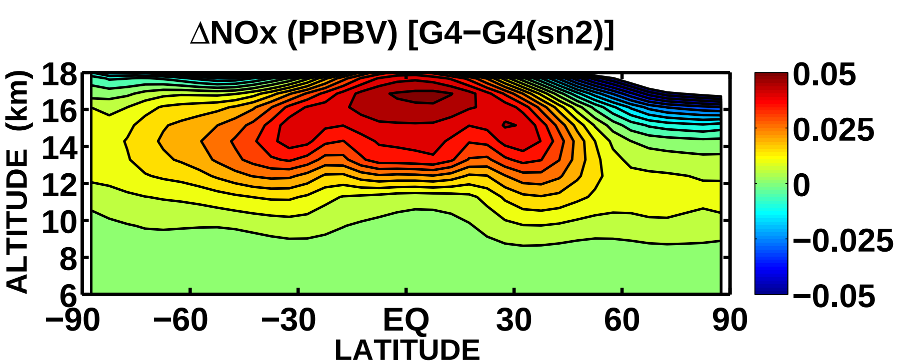

Figure S8. G4-G4(sn2) anomalies of NO+NO_2 mixing ratios in the upper troposphere and lowermost stratosphere, from ULAQ-CCM (b) (time average 2040-2049) (ppbv). The contour line increment is 0.005 ppbv. The sensitivity case G4-sn2 keeps temperature fixed at RCP4.5 values in the chemistry module.

References

Andrews, A. E., Boering, K. A., Daube, B. C., Wofsy, S. C., Loewenstein, M., Jost, H., Podolske, J. R., Webster, C. R., Herman, R. L., Scott, D. C., Flesch, G. J., Moyer, E. J., Elkins, J. W., Dutton, G. S., Hurst, D. F., Moore, F. L., Ray, E. A., Romashkin, P. A., and Strahan, S. E.: Mean ages of stratospheric air derived from in situ observations of CO_2, CH_4, and N_2O, Journal of Geophysical Research: Atmospheres, 106, 32 295–32 314, doi:10.1029/2001JD000465, http://dx.doi.org/10.1029/2001JD000465, 2001.

Austin, J., Shindell, D., Beagley, S. R., Brühl, C., Dameris, M., Manzini, E., Nagashima, T., Newman, P., Pawson, S., Pitari, G., Rozanov, E., Schnadt, C., and Shepherd, T. G.: Uncertainties and assessments of chemistry-climate models of the stratosphere, Atmospheric Chemistry and Physics, 3, 1–27, doi:10.5194/acp-3-1-2003, http://www.atmos-chem-phys.net/3/1/2003/, 2003.

Engel, A., Mobius, T., Bonisch, H., Schmidt, U., Heinz, R., Levin, I., Atlas, E., Aoki, S., Nakazawa, T., Sugawara, S., Moore, F., Hurst, D., Elkins, J., Schauffler, S., Andrews, A., and Boering, K.: Age of stratospheric air unchanged within uncertainties over the past 30 years, Nature Geosci, 2, 28–31, http://dx.doi.org/10.1038/ngeo388, 2009.

Grooss, J. and Russell III, J. M.: Technical note: A stratospheric climatology for O_3, H_2O, CH_4, NO_x, HCl and HF derived from HALOE measurements, Atmospheric Chemistry and Physics, 5, 2797–2807, doi:10.5194/acp-5-2797-2005, http://www.atmos-chem-phys.net/5/2797/2005/, 2005.

Strahan, S. E., Douglass, A. R., Stolarski, R. S., Akiyoshi, H., Bekki, S., Braesicke, P., Butchart, N., Chipperfield, M. P., Cugnet, D., Dhomse, S., Frith, S. M., Gettelman, A., Hardiman, S. C., Kinnison, D. E., Lamarque, J.-F., Mancini, E., Marchand, M., Michou, M., Morgenstern, O., Nakamura, T., Olivie, D., Pawson, S., Pitari, G., Plummer, D. A., Pyle, J. A., Scinocca, J. F., Shepherd, T. G., Shibata, K., Smale, D., Teyssedre, H., Tian, W., and Yamashita, Y.: Using transport diagnostics to understand chemistry climate model ozone simulations, Journal of Geophysical Research: Atmospheres, 116, n/a–n/a, doi:10.1029/2010JD015360, http://dx.doi.org/10.1029/2010JD015360, d17302, 2011.

Urban, J., Pommier, M., Murtagh, D. P., Santee, M. L., and Orsolini, Y. J.: Nitric acid in the stratosphere based on Odin observations from 2001 to 2009 ? Part 1: A global climatology, Atmospheric Chemistry and Physics, 9, 7031–7044, doi:10.5194/acp-9-7031-2009, http://www.atmos-chem-phys.net/9/7031/2009/, 2009.

Worden, J., Kulawik, S., Frankenberg, C., Payne, V., Bowman, K., Cady-Peirara, K., Wecht, K., Lee, J.-E., and Noone, D.: Profiles of CH_4, HDO, H_2O, and N_2O with improved lower tropospheric vertical resolution from Aura TES radiances, Atmospheric Measurement Techniques, 5, 397–411, doi:10.5194/amt-5-397-2012, http://www.atmos-meas-tech.net/5/397/2012/, 2012.